Bone 97 (2017) 43–48

Contents lists available at ScienceDirect

Bone

journal homepage: www.elsevier.com/locate/bone

Full Length Article

Quantitative *in vivo* assessment of bone microarchitecture in the human knee using HR-pQCT

Andres Kroker [a,c], Ying Zhu [a,c], Sarah L. Manske [a,c], Rhamona Barber [b], Nicholas Mohtadi [b,c], Steven K. Boyd [a,c,*]

[a] Department of Radiology, Cumming School of Medicine, University of Calgary, Canada
[b] University of Calgary Sport Medicine Centre, University of Calgary, Canada
[c] McCaig Institute for Bone and Joint Health, University of Calgary, Canada

ARTICLE INFO

Article history:
Received 8 September 2016
Revised 10 December 2016
Accepted 25 December 2016
Available online 27 December 2016

Keywords:
HR-pQCT
Bone microarchitecture
Knee
Osteophyte
Anterior cruciate ligament
Bone mineral density

ABSTRACT

Objective: High-resolution peripheral quantitative computed tomography (HR-pQCT) is a novel imaging modality capable of visualizing bone microarchitecture *in vivo* at human peripheral sites such as the distal radius and distal tibia. This research has extended the technology to provide a non-invasive assessment of bone microarchitecture at the human knee by establishing new hardware, imaging protocols and data analysis.
Design: A custom leg holder was developed to stabilize a human knee centrally within a second generation HR-pQCT field of view. Five participants with anterior cruciate ligament reconstructions had their knee joint imaged in a continuous scan of 6 cm axially. The nominal isotropic voxel size was 60.7 μm. Bone mineral density and microarchitecture were assessed within the weight-bearing regions of medial and lateral compartments of the knee at three depths from the weight-bearing articular bone surface, including both the cortical and trabecular bone regions.
Results: Scan duration was approximately 18 min per knee and produced 5 GB of projection data and 10 GB of reconstructed image data (2304 × 2304 image matrix, 1008 slices). Motion during the scan was minimized by the leg holder and was similar in magnitude as a scan of the distal tibia. Bone mineral density and microarchitectural parameters were assessed for 16 volumes of interest in the tibiofemoral joint.
Conclusions: This is a new non-invasive *in vivo* assessment tool for bone microarchitecture in the human knee that provides an opportunity to gain insight into normal, injured and surgically reconstructed human knee bone architecture in cross-sectional or longitudinal studies.

1. Introduction

Bone microarchitecture adaptation in the human knee may play a role in the increased risk of developing post-traumatic osteoarthritis (OA) associated with an anterior cruciate ligament (ACL) tear [1]. After an ACL injury significant bone loss has been identified in the injured knee [2,3]. Whereas in animal models these changes have been associated with underlying bone microarchitecture [4,5], to date it has not been possible to explore bone microarchitecture in the human knee.

Bone microarchitecture can be non-invasively assessed using micro computed tomography (μCT) with resolutions less than 10 μm, but its applications have been limited to bone biopsies or animal models due to the small field of view (FOV) [6,7]. Clinical CT systems provide larger FOV and fast, non-invasive imaging of whole joints *in vivo*, but the resolution is insufficient to provide bone microarchitectural information [8–11]. Magnetic resonance imaging (MRI) allows for bone imaging without ionizing radiation, however, both its dependency on fatty bone marrow for contrast and insufficient spatial resolution limit its use for trabecular or cortical bone microarchitectural analysis [12–15]. Bridging the gap between μCT and clinical CT, high-resolution peripheral quantitative computed tomography (HR-pQCT) was introduced in 2005. It is an established research tool for studying *in vivo* human bone microarchitecture by providing insight into skeletal changes associated with diseases such as osteoporosis [16,17]. However, measurements were confined to peripheral sites such as the distal radius and distal tibia because first generation machines had a small gantry diameter and limited length allowance.

Recently, a second generation HR-pQCT scanner (XtremeCT II, Scanco Medical) was introduced that can provide images with a 61 μm nominal isotropic voxel size and 95 μm spatial resolution. This new technology has been shown to accurately measure human bone microarchitectural parameters at the standard radius and tibia skeletal sites [18]. It has a longer and wider gantry which provides a larger FOV. This new design has potential to accommodate more proximal joints at the extremities, such as the knee and elbow.

* Corresponding author at: McCaig Institute for Bone and Joint Health, University of Calgary, 3280 Hospital Drive NW, Calgary, Alberta T2N 4Z6, Canada.
E-mail addresses: akroker@ucalgary.ca (A. Kroker), yingzhu@ucalgary.ca (Y. Zhu), smanske@ucalgary.ca (S.L. Manske), rsg.barber@ucalgary.ca (R. Barber), mohtadi@ucalgary.ca (N. Mohtadi), skboyd@ucalgary.ca (S.K. Boyd).

http://dx.doi.org/10.1016/j.bone.2016.12.015
8756-3282/

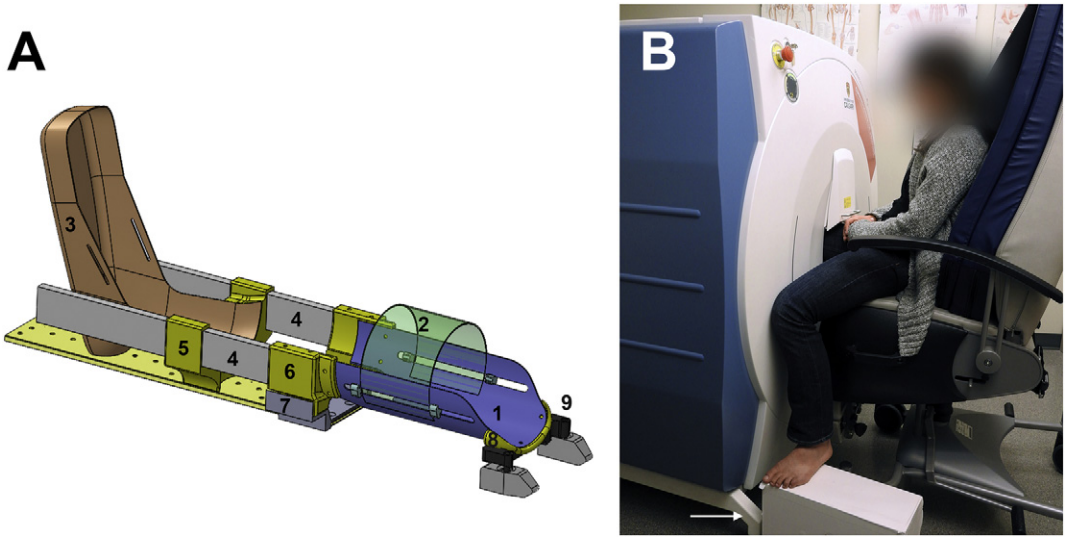

Fig. 1. Schematic of the leg holder and subject positioning. Leg holder schematics (A): Two carbon fiber tube segments, a knee support (1) and a knee cap (2), to stabilize the knee within the FOV. A carbon fiber foot holder (3) slides along the two side bars (4) to adjust for a range of human leg lengths. Three plastic adapters were rapid-prototyped to fit in custom shapes: a foot adapter (5) to support and slide the foot holder, a calf adapter (6) to support and dock 1 and 4 onto a metal calf dock (7), and a thigh adapter (8) to dock the knee support (1) on the proximal end onto a metal thigh dock (9). Subject positioning (B): The fully extended knee is inserted into the HR-pQCT gantry while the subject is sitting in an upright position and the opposite leg is positioned to the side and rests on a stool (arrow).

The aim of this study was to develop a non-invasive assessment tool for bone microarchitecture in the human knee. We describe the data acquisition process and analysis of an *in vivo* human knee scan protocol using a second generation of HR-pQCT. The approach was applied to the reconstructed knee of five volunteers who had unilateral anterior cruciate ligament (ACL) reconstructions to demonstrate the potential of this method to capture joint changes due to disease or surgical interventions.

2. Methods

2.1. Custom leg holder

In vivo HR-pQCT scans require strict control of participant motion for the duration of image acquisition. To reduce motion artifacts, a custom leg holder was developed (Fig. 1A) to stabilize the participant's knee centrally in the FOV (diameter: 140 mm; axial depth: 200 mm). The leg holder consisted of two carbon fiber tube segments that maintained a fixed knee position within the FOV. An adjustable carbon fiber foot piece allowed fitting legs of different lengths into the scanner while maintaining an optimal knee position within the FOV by sliding along two bars (rails) at each side of the holder. Three plastic adapters (VeroWhite RGD525, Stratasys, Eden Prairie, MN, USA) were built by rapid-prototyping (Objet Connex, Stratasys, Eden Prairie, MN, USA) to ensure support of the knee and alignment in the scanner (at the foot, calf and thigh).

2.2. Participants

Five volunteer participants with unilateral ACL reconstructions (6.5 ± 0.45 years prior) were recruited from a cohort that participated in a randomized controlled surgery trial [19]. Participants were aged between 20.9 and 43.1 years, and included three males and two females. For each participant, we scanned the reconstructed knee (four left, one right). Body weight and height were measured prior to scanning. Knee circumference was measured posteriorly of the patella and knee height was measured as the height of the patella center in upright stance. All participants gave informed consent prior to entering the study. This study was approved by the University of Calgary Conjoint Health Research Ethics Board (Ethics ID 20966) and procedures followed were in accordance with the Helsinki Declaration of 1975, as revised in 2000.

2.3. HR-pQCT imaging

Imaging of the knee was performed on the second generation HR-pQCT (XtremeCT II, Scanco Medical, Brüttisellen, Switzerland). Participants were placed in an upright sitting position with the target leg in full extension inside the HR-pQCT gantry. The opposite leg was resting comfortably on a side foot stool (Fig. 1B). The x-ray settings were adjusted to accommodate the larger girth of the knee joint compared to a

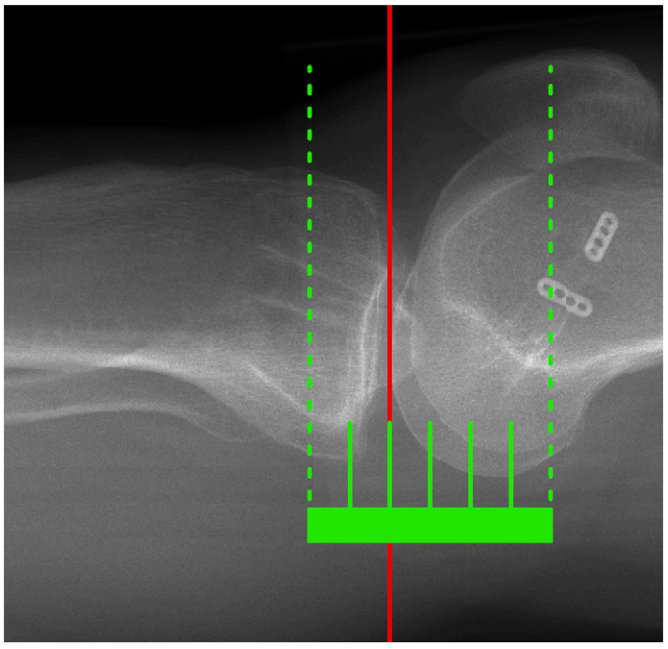

Fig. 2. Scout x-ray view. The solid vertical reference line is defined as most distal point of femoral condyle. The scan occurs between the dashed lines. The transitions between the six image sections, acquired separately and merged into the final large dataset, are depicted.

Fig. 3. Typical segmented knee bones (femur, tibia, patella). Arrows highlight the ACL reconstruction tunnel in the tibia.

radius or tibia by increasing the integration time (68 kVp, 1470 μA, 100 ms integration time, 156 mAs per stack (168 slices)). A total of 1008 axial slices with an image matrix of 2304 × 2304 were collected at a nominal isotropic voxel size of 60.7 μm. This resulted in an image volume measuring 61.2 mm in length and 139.9 × 139.9 mm in the axial plane.

The scan region was defined by the HR-pQCT operator placing a reference line at the most distal point of the femoral condyle in a scout view image acquired in the sagittal plane (Fig. 2). The scan started 20.4 mm distally from the reference line and ended 40.8 mm proximally, capturing approximately 40 mm of the distal femur and 20 mm of the proximal tibia. This scan region included the articular joint surfaces of both the tibia and femur as well as the reconstruction tunnels within those bones (Fig. 3).

2.4. X-ray

Standard postero-anterior weight-bearing, lateral and skyline patellar x-ray views were acquired at the University of Calgary Sport Medicine Centre.

2.5. Data analysis

Data analysis included three major steps: image segmentation, volume of interest (VOI) definition, and bone mineral density and bone morphological analysis.

2.5.1. Image segmentation

The goal of the image segmentation was to define the periosteal and endosteal surfaces for each bone. This was achieved using an adaptation of the dual-thresholding method that has been established for the segmentation of standard radius and tibia HR-pQCT scans [20] (IPL v5.42, Scanco Medical). After manually extracting the bone of interest (distal femur or proximal tibia), the periosteal and endosteal bone surfaces were defined by the dual-thresholding method. A minimal cortical thickness of 0.36 mm was defined as is standard in the radius and tibia scans, and the subchondral cortical plate was defined as the volume between the periosteal and endosteal bone surfaces.

2.5.2. Volume of interest definition

The weight-bearing region of each condyle was defined manually by interactively placing points along the margins using a 3D visualization of the articular surfaces in a custom software package (blSurfaceViewer, University of Calgary). The area on the articular surface was defined by fitting a polynomial curve through these points (Fig. 4A, B), and then each surface was projected into the 3D knee bones to define three depths (periarticular, shallow layer: 0.0–2.5 mm, mid layer: 2.5–5.0 mm, deep layer: 5.0–7.5 mm) used for quantitative analysis (Fig. 4C, D). The definition of these VOIs follows the work of Johnston et al. for clinical CT scans of the human knee [8,11]. For each condyle, a cortical VOI was defined as the space between the periosteal and endosteal bone surface contours. This process produced four VOIs per knee condyle, resulting in a total of 16 VOIs in the tibiofemoral joint. The cortical VOI was subtracted from the three trabecular layers to separate between cortical and trabecular bone in the bone microarchitectural analysis. Thus, the shallow layer started below the cortex instead of at the joint surface.

2.5.3. Bone parameter analysis

Within each VOI, bone morphology was assessed following methods developed for radius and tibia analysis by HR-pQCT (IPL v5.42, Scanco Medical) [18]. Trabecular VOIs were assessed for BMD (Tb.BMD; mg HA/cm^3), trabecular thickness (Tb.Th; mm), trabecular separation (Tb.Sp; mm), trabecular number (Tb.N; mm^{-1}) and trabecular bone volume fraction (Tb.BVTV; %), while the cortical VOIs were assessed for cortical BMD (Ct.BMD; mg HA/cm^3), cortical thickness (Ct.Th; mm) and cortical porosity (Ct.Po; %). Cortical BMD was assessed including the cortical pores [18].

3. Results

3.1. HR-pQCT scanning

All five participants had their knees successfully scanned with HR-pQCT. The scanner's gantry size and FOV limited scanning to knees that had a maximal circumference of 42 cm and a height of 52 cm to

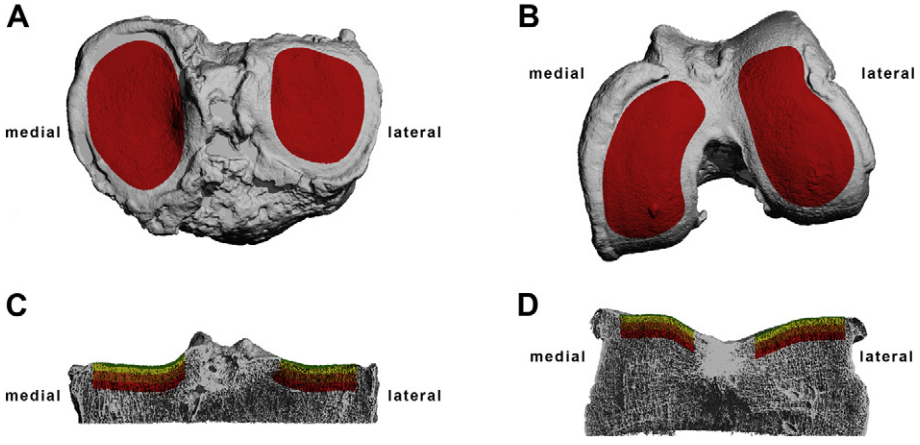

Fig. 4. Definition of weight-bearing regions. After selection of points, the weight-bearing region is defined for the tibia (A) and the femur (B). Three layers define the VOIs at the tibia (C) and femur (D) as shown in these coronal cuts. The layers are defined as shallow (0.0 mm–2.5 mm), mid (2.5 mm–5.0 mm) and deep (5.0 mm–7.5 mm). The subchondral bone plate is defined within the weight-bearing region. Note the presence of osteophytes along the edges of the articulated surfaces of both tibit (A) and femur (B). The coronal cut through the distal femur (D) highlights the bone microarchitecture of osteophytes.

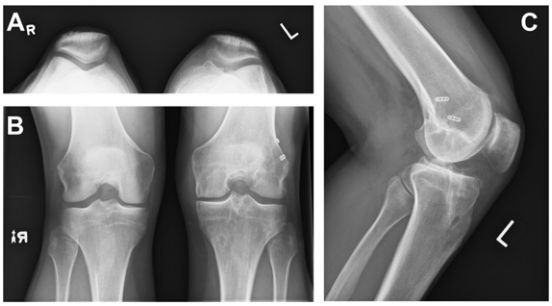

Fig. 5. Planar X-rays. Planar x-rays in the skyline (A), frontal (B) and lateral view with 30 degrees flexion (C) are shown for the same knee as presented in Fig. 3.

the center of the patella in upright stance. One of the participants had a patella protruding about 1 mm out of the FOV.

Each knee scan took 18 min and produced 5 GB of raw projection data. Software developments were provided by the manufacturer (Scanco Medical) so that all data transfers from HR-pQCT to workstation occurred after completion of the tomographic acquisition to minimize the participant's time in the scanner. Image reconstruction took approximately 2.5 h when dividing the projection data into 24 batches, processing them in parallel on four server blades (HP Integrity BL860c i2 Sever Blade, HP, Palo Alto, CA, USA) and two separate workstations (HP Integrity rx2800 i2 Server, HP). The reconstructed 3D image data file size was 10 GB per knee scan. The estimated effective radiation dose for each knee scan was less than 50 μSv as assessed by the manufacturer's software.

The leg holder accurately positioned the knee in the center of the FOV reducing motion over the duration of the scan to similar magnitude as the much shorter (2 min) standard distal tibia HR-pQCT scans. Each knee scan was created by repeatedly acquiring six batches of 168 image slices resulting in a final knee image with a total of 1008 slices. Small discontinuities were visible in the segmented images at intervals of 168 slices.

3.2. Bone morphology

The 16 defined VOIs resulted in 72 quantitative measurements per knee. In addition to the quantitative measurements, qualitative visualization of the entire knee revealed the presence of osteophytes at the edges of the articular joint surfaces. These are evident in 3D images of the knee (Fig. 4), but are difficult to identify in standard planar x-ray images (Fig. 5). Cortical thickness maps of the weight-bearing regions show the distribution of the parameter throughout the medial and lateral compartment for both tibia and femur (Fig. 6A, B). All bone microarchitecture parameters are summarized in Tables 1 and 2.

4. Discussion

This study describes a protocol for assessing bone microarchitecture in the human knee *in vivo* using the second generation HR-pQCT. A great benefit of HR-pQCT is the low effective radiation dose, which is similar in magnitude to a chest x-ray. The strength of our approach is that it provides a non-invasive measure that has potential to be applied for assessing longitudinal bone microarchitecture changes in the human knee. This technology provides a novel opportunity to explore how bone microarchitecture is affected in the human knee following an injury or disease.

There are some challenges and limitations to our approach. Physically, the size of the HR-pQCT gantry and FOV currently limit the size (girth) of knees that can be scanned resulting in the knees of large (overweight or muscular) or tall individuals possibly not fitting (Table 3). A simple measure of knee girth prior to scanning can ensure the appropriateness of an individual, and we used 42 cm girth as a maximum. Another challenge of our technique is the long scan duration (18 min), which has practical limitations. It is critical to ensure comfort of the participant and stability of the joint during the scan to minimize motion artifacts, which was quite feasible as we gained experience. Finally, the enormous data file sizes present a challenge, especially if the computing support for the scanner does not include multiple blade servers and workstations to share the computational load. Without parallel processing across multiple blades or workstations (*i.e.* single workstation) the reconstruction time was 13.3 h.

In comparison to standard radius or tibia scans conducted normally by HR-pQCT, data analysis for the knee is complex as the images are six times larger in size, a set of subject-specific VOIs is required, and the subchondral cortical bone can be thin and highly variable in thickness. We defined several VOIs that followed previous work using clinical CT [8], as these are well suited to capture morphological features of the knee bones. However, there is significant variation in how the etiology of OA may manifest in the knee, and it is entirely possible that the VOIs we selected could miss important findings. The most evident bone morphological aspect of OA on x-ray is the presence of osteophytes. It is therefore of great advantage that our approach provides a full 3D model of each knee that can be examined. It is likely that future studies will further customize VOI definitions to suit their specific research question. Using the current VOIs, we are now using our technique to conduct research investigating bone morphology in ACL-reconstructed knees, as well as longitudinal studies investigating bone changes after an acute ACL injury. The large 3D datasets provide an unprecedented opportunity to explore bone microarchitecture in the knee.

The microarchitectural information indicates differences in bone as a function of depth, and between compartments, although a more extensive study should be performed to establish microarchitecture trends in normal and injured joints. The reported results in Tables 1 and 2 fall

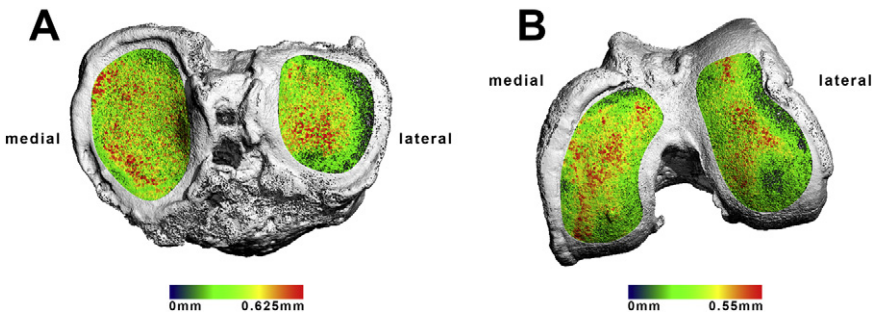

Fig. 6. Cortical thickness map and segmented knee bones. (A) Cortical thickness maps of the weight bearing surfaces of the tibia, and (B) cortical thickness maps of the weight bearing surfaces of the femur.

Table 1
Morphological analysis in the two compartments of each bone. Within each compartment the three layers examined are the shallow, mid and deep layers (n = 5).

Trabecular bone microarchitectural parameters								
Parameter	Bone	Compartment	Shallow layer		Mid layer		Deep layer	
			Min	Max	Min	Max	Min	Max
Tb.BMD [mg HA/cm^3]	Femur	Lateral	264.1	350.8	223.8	283.9	198.9	261.7
		Medial	219.0	324.6	178.5	251.6	149.7	213.2
	Tibia	Lateral	252.2	354.4	186.8	263.7	137.4	185.6
		Medial	298.0	390.2	235.7	306.0	178.1	210.3
Tb.Th [mm]	Femur	Lateral	0.243	0.313	0.211	0.281	0.204	0.283
		Medial	0.227	0.281	0.217	0.227	0.201	0.220
	Tibia	Lateral	0.234	0.311	0.228	0.292	0.210	0.252
		Medial	0.291	0.332	0.255	0.322	0.241	0.275
Tb.Sp [mm]	Femur	Lateral	0.298	0.439	0.348	0.522	0.393	0.594
		Medial	0.323	0.592	0.391	0.761	0.510	0.877
	Tibia	Lateral	0.362	0.576	0.474	0.731	0.583	0.901
		Medial	0.279	0.493	0.404	0.652	0.560	0.831
Tb.N [mm^{-1}]	Femur	Lateral	2.10	2.74	1.82	2.52	1.62	2.29
		Medial	1.71	2.66	1.35	2.35	1.17	1.94
	Tibia	Lateral	1.74	2.53	1.37	1.99	1.12	1.67
		Medial	1.99	2.82	1.54	2.24	1.23	1.72
Tb.BVTV [%]	Femur	Lateral	37.9	55.4	30.9	41.8	25.8	37.4
		Medial	29.1	50.6	22.7	35.3	18.7	28.0
	Tibia	Lateral	34.8	52.8	26.1	37.5	18.8	24.6
		Medial	44.0	63.2	33.5	46.0	23.6	29.6

within the range of previously reported bone microarchitectural parameters from *ex vivo* studies [21–23]. Some of the presented parameters (Tb.N, femoral Tb.Th) are higher in this study, however our study population was younger which likely affected the range due to higher bone quality at a younger age [22,24]. With our limited results (n = 5), when comparing Tb.BMD and Tb.N of the knee to normative curves [25] of these parameters for the distal tibia and radius, one can see that the presented ranges at the shallow layer are similar to the distal tibia of younger adults aged 20 years, while the deeper layers are more representative of the distal tibia of older adults aged above 80 years. However, it is difficult to draw conclusions due to the heterogeneity of bone microarchitecture at different skeletal sites [26–28]. A study with a larger sample is ongoing.

Our HR-pQCT scanning technique was tested on five previously injured knees with varying degrees of osteoarthritis development, and the evaluation of the articular surfaces (Fig. 4) revealed the presence of osteophytes. From these five knees, the one with pronounced osteophytes was from the participant with the longest time between injury and surgery (Tables 3, 4). In the future, it would be valuable to develop quantitative methods to assess structure, size, distribution, and the underlying bone microarchitecture of osteophytes as they are important part of the etiology of knee osteoarthritis. We are also particularly interested in the tunnels created for the reconstructive surgery as we have qualitatively noted bone adaptations in the tunnel wall. Future studies may evaluate changes in tunnel structure, healing of the bone along the drill hole, and integration of the graft into the bone. While it would be ideal to address all of these research interests in a single knee scan, the challenges in terms of scanning time and dataset sizes will likely require a focused study design. We are excited about the potential for HR-pQCT to study bone microarchitecture in knees and have completed preliminary work extending the technique to other joints such as the elbow [29].

Overall, it is clear that the measurement of knee microarchitecture is better suited for research studies than clinical applications. Nevertheless, the approach was highly successful for all five of our subjects, and produced excellent quality microarchitectural information on their knees. Ongoing work includes a cross-sectional study comparing the bone microarchitecture of 35 people with three different ACL reconstruction surgeries, and a longitudinal study of bone adaptation in the first eight months following an acute ACL injury. The importance of bone changes in knee injuries has been established in animal models, and it is now possible to extend these studies to human research. Hopefully, this work will support the development of effective interventions and treatments to improve knee outcomes.

5. Conclusion

We have demonstrated a technique to image human knees with HR-pQCT *in vivo*. We developed a custom leg holder that minimized motion artifacts, and defined VOIs and a microarchitectural analysis protocol to characterize the weight-bearing regions of the knee.

Table 2
Subchondral cortical bone analysis in the two compartments of each bone (n = 5).

Cortical bone microarchitectural parameters				
Parameter	Bone	Compartment	Min	Max
Ct.BMD [mg HA/cm^3]	Femur	Lateral	518.4	596.3
		Medial	548.4	628.0
	Tibia	Lateral	545.8	672.1
		Medial	555.8	639.0
Ct.Th [mm]	Femur	Lateral	0.315	0.380
		Medial	0.332	0.394
	Tibia	Lateral	0.352	0.421
		Medial	0.389	0.467
Ct.Po [%]	Femur	Lateral	23.5	37.2
		Medial	24.4	30.0
	Tibia	Lateral	17.6	31.8
		Medial	19.6	27.6

Table 3
Anthropometry of participants.

Anthropometry					
Participant	1	2	3	4	5
Height [cm]	181.2	170.9	187.5	164.6	171.9
Weight [kg]	90.8	81.0	94.7	68.9	84.4
Age [years]	27.8	40.1	43.1	20.9	27.3
Sex	Male	Male	Male	Female	Female
Injured knee	Left	Left	Left	Left	Right
Circumference left knee [cm]	41.2	41.0	41.8	35.7	45.0
Circumference right knee [cm]	41.0	40.9	41.8	37.0	45.3
Height left knee [cm]	53.8	49.3	51.0	46.3	49.8
Height right knee [cm]	54.2	49.5	52.5	46.2	50.1

Table 4
Injury and intervention data of participants. Times are with respect to the scan date.

Injury and intervention data					
Participant	1	2	3	4	5
Time since injury	7 yrs, 4 m, 18 d	7 yrs, 11 m, 6 d	13 yrs, 11 m, 18 d	7 yrs, 1 m, 8 d	7 yrs, 6 m, 7 d
Time since reconstruction	6 yrs, 7 m, 18 d	6 yrs, 0 m, 19 d	7 yrs, 0 m, 27 d	6 yrs, 1 m, 19 d	6 yrs, 8 m, 17 d
Type of graft	Hamstring autograft	Hamstring autograft	Hamstring autograft	Hamstring autograft	Hamstring autograft
Type of reconstruction	Double bundle	Double bundle	Double bundle	Single bundle	Double bundle

Contributions

Authors roles: Study design: AK, YZ, SLM, RB, NM, SKB. Data acquisition: AK, YZ, SLM. Data analysis: AK, SLM, NM, SKB. Recruitment: RB. Method development: AK, YZ, SLM, SKB. Reconstructive surgeries: NM. Drafting manuscript: AK, SKB. All authors contributed to manuscript revisions and approved the final, submitted version. AK, SLM, and SKB take responsibility for the integrity of the data analysis.

Role of the funding source.

The study was supported by the following funding sources: Natural Sciences and Engineering Research Council (NSERC) Discovery Grant, Canada Foundation for Innovation, University of Calgary Eyes High. None of the funding sources were involved in study design, data collection, data analysis and interpretation, writing of the manuscript, or the decision to submit the manuscript for publication.

Conflict of interest statement

None of the authors has a conflict of interest to declare.

Acknowledgements

We would like to acknowledge Anne Cooke, Taryn Grant, and Duncan Raymond for technical support. We would like to thank Stefan Hämmerle from Scanco Medical for hardware support, and Kourosh Zareinia, Peter Byrne and Robert Scorey for manufacturing support.

Appendix A. Supplementary data

Supplementary data to this article can be found online at http://dx.doi.org/10.1016/j.bone.2016.12.015.

References

[1] L.S. Lohmander, P.M. Englund, L.L. Dahl, E.M. Roos, The long-term consequence of anterior cruciate ligament and meniscus injuries: osteoarthritis, Am. J. Sports Med. 35 (2007) 1756–1769, http://dx.doi.org/10.1177/0363546507307396.
[2] H. Sievänen, P. Kannus, A. Heinonen, P. Oja, I. Vuori, Bone mineral density and muscle strength of lower extremities after long-term strength training, subsequent knee ligament injury and rehabilitation: a unique 2-year follow-up of a 26-year-old female student, Bone 15 (1994) 85–90, http://dx.doi.org/10.1016/8756-3282(94)90896-6.
[3] P.P.Y. Lui, Y.Y. Cheng, S.H. Yung, A.S.L. Hung, K.M. Chan, A randomized controlled trial comparing bone mineral density changes of three different ACL reconstruction techniques, Knee 19 (2012) 779–785, http://dx.doi.org/10.1016/j.knee.2012.02.005.
[4] B.A. Christiansen, M.J. Anderson, C.A. Lee, J.C. Williams, J.H.N. Yik, D.R. Haudenschild, Musculoskeletal changes following non-invasive knee injury using a novel mouse model of post-traumatic osteoarthritis, Osteoarthr. Cartil. 20 (2012) 773–782, http://dx.doi.org/10.1016/j.joca.2012.04.014.
[5] S.K. Boyd, R. Müller, R.F. Zernicke, Mechanical and architectural bone adaptation in early stage experimental osteoarthritis, J. Bone Miner. Res. Off. J. Am. Soc. Bone Miner. Res. 17 (2002) 687–694, http://dx.doi.org/10.1359/jbmr.2002.17.4.687.
[6] K.K. Nishiyama, G.M. Campbell, R.J. Klinck, S.K. Boyd, Reproducibility of bone microarchitecture measurements in rodents by in vivo micro-computed tomography is maximized with three-dimensional image registration, Bone 46 (2010) 155–161, http://dx.doi.org/10.1016/j.bone.2009.09.023.
[7] P. Ruegsegger, B. Koller, R. Muller, A microtomographic system for the nondestructive evaluation of bone architecture, Calcif. Tissue Int. 58 (1996) 24–29, http://dx.doi.org/10.1007/s002239900006.
[8] J.D. Johnston, B.A. Masri, D.R. Wilson, Computed tomography topographic mapping of subchondral density (CT-TOMASD) in osteoarthritic and normal knees: methodological development and preliminary findings, Osteoarthr. Cart 17 (2009) 1319–1326, http://dx.doi.org/10.1016/j.joca.2009.04.013.
[9] N.J. Emerson, A.C. Offiah, G.C. Reilly, M.J. Carré, Patient-specific finite element modelling and validation of porcine femora in torsion, Strain 49 (2013) 212–220, http://dx.doi.org/10.1111/str.12029.
[10] W. Burnett, S. Kontulainen, C. McLennan, D. Hazel, C. Talmo, D. Hunter, D. Wilson, J. Johnston, Patella bone density is lower in knee osteoarthritis patients experiencing moderate-to-severe pain at rest, J. Musculoskelet. Neuronal Interact. 16 (2016) 33–39.
[11] J.D. Johnston, C.E. McLennan, D.J. Hunter, D.R. Wilson, In vivo precision of a depth-specific topographic mapping technique in the CT analysis of osteoarthritic and normal proximal tibial subchondral bone density, Skelet. Radiol. 40 (2011) 1057–1064, http://dx.doi.org/10.1007/s00256-010-1001-6.
[12] J.M. Patsch, A.J. Burghardt, G. Kazakia, S. Majumdar, Noninvasive imaging of bone microarchitecture: Patsch et al, Ann. N. Y. Acad. Sci. 1240 (2011) 77–87, http://dx.doi.org/10.1111/j.1749-6632.2011.06282.x.
[13] R. Krug, J. Carballido-Gamio, S. Banerjee, A.J. Burghardt, T.M. Link, S. Majumdar, In vivo ultra-high-field magnetic resonance imaging of trabecular bone microarchitecture at 7 T, J. Magn. Reson. Imaging 27 (2008) 854–859, http://dx.doi.org/10.1002/jmri.21325.
[14] G.A. Ladinsky, F.W. Wehrli, Noninvasive assessment of bone microarchitecture by MRI, Curr. Osteoporos. Rep. 4 (2006) 140–147.
[15] W.C. Bae, S. Patil, R. Biswas, S. Li, E.Y. Chang, S. Statum, D.D. D'Lima, C.B. Chung, J. Du, Magnetic resonance imaging assessed cortical porosity is highly correlated with μCT porosity, Bone 66 (2014) 56–61, http://dx.doi.org/10.1016/j.bone.2014.06.004.
[16] K.K. Nishiyama, E. Shane, Clinical imaging of bone microarchitecture with HR-pQCT, Curr. Osteoporos. Rep. 11 (2013) 147–155, http://dx.doi.org/10.1007/s11914-013-0142-7.
[17] R. Krug, A.J. Burghardt, S. Majumdar, T.M. Link, High-resolution imaging techniques for the assessment of osteoporosis, Radiol. Clin. N. Am. 48 (2010) 601–621, http://dx.doi.org/10.1016/j.rcl.2010.02.015.
[18] S.L. Manske, Y. Zhu, C. Sandino, S.K. Boyd, Human trabecular bone microarchitecture can be assessed independently of density with second generation HR-pQCT, Bone 79 (2015) 213–221, http://dx.doi.org/10.1016/j.bone.2015.06.006.
[19] N. Mohtadi, D. Chan, R. Barber, E. Oddone Paolucci, A randomized clinical trial comparing patellar tendon, hamstring tendon, and double-bundle ACL reconstructions: patient-reported and clinical outcomes at a minimal 2-year follow-up, Clin. J. Sport Med. 25 (2015) 321–331, http://dx.doi.org/10.1097/JSM.0000000000000165.
[20] H.R. Buie, G.M. Campbell, R.J. Klinck, J.A. MacNeil, S.K. Boyd, Automatic segmentation of cortical and trabecular compartments based on a dual threshold technique for in vivo micro-CT bone analysis, Bone 41 (2007) 505–515, http://dx.doi.org/10.1016/j.bone.2007.07.007.
[21] J.D. Johnston, B.A. Masri, D.R. Wilson, Computed tomography topographic mapping of subchondral density (CT-TOMASD) in osteoarthritic and normal knees: methodological development and preliminary findings, Osteoarthr. Cartil. 17 (2009) 1319–1326, http://dx.doi.org/10.1016/j.joca.2009.04.013.
[22] V. Patel, A.S. Issever, A. Burghardt, A. Laib, M. Ries, S. Majumdar, MicroCT evaluation of normal and osteoarthritic bone structure in human knee specimens, J. Orthop. Res. 21 (2003) 6–13.
[23] B.C. Roberts, D. Thewlis, L.B. Solomon, G. Mercer, K.J. Reynolds, E. Perilli, Systematic mapping of the subchondral bone 3D microarchitecture in the human tibial plateau: variations with joint alignment, J. Orthop. Res. (2016) (http://onlinelibrary.wiley.com/doi/10.1002/jor.23474/full (accessed December 8, 2016)).
[24] H.M. MacDonald, K.K. Nishiyama, J. Kang, D.A. Hanley, S.K. Boyd, Age-related patterns of trabecular and cortical bone loss differ between sexes and skeletal sites: a population-based HR-pQCT study, J. Bone Miner. Res. 26 (2011) 50–62, http://dx.doi.org/10.1002/jbmr.171.
[25] L.A. Burt, Z. Liang, T.T. Sajobi, D.A. Hanley, S.K. Boyd, Sex- and site-specific normative data curves for HR-pQCT, J. Bone Miner. Res. (2016)http://dx.doi.org/10.1002/jbmr.2873.
[26] M. Amling, S. Herden, M. Pösl, M. Hahn, H. Ritzel, G. Delling, Heterogeneity of the skeleton: comparison of the trabecular microarchitecture of the spine, the iliac crest, the femur, and the calcaneus, J. Bone Miner. Res. Off. J. Am. Soc. Bone Miner. Res. 11 (1996) 36–45, http://dx.doi.org/10.1002/jbmr.5650110107.
[27] T. Hildebrand, P. Rüegsegger, Quantification of bone microarchitecture with the structure model index, Comput. Methods Biomech. Biomed. Engin. 1 (1997) 15–23, http://dx.doi.org/10.1080/01495739708936692.
[28] A. Cohen, D.W. Dempster, R. Mueller, X.E. Guo, T.L. Nickolas, X.S. L., X.H. Zahng, A.J. Wirth, G.H.V. Lenthe, T. Kohler, D.J. Mcmahon, H. Zhou, M.R. Rubin, Assessment of trabecular and cortical architecture and mechanical competence of bone by high-resolution peripheral computed tomography: comparison with transiliac bone biopsy, Osteoporos. Int. 21 (2010) 263–273, http://dx.doi.org/10.1007/s00198-009-0945-7.
[29] K.E. Archibold, S.L. Manske, K.A. Hildebrand, S.K. Boyd, Evaluation of primary elbow osteoarthritis using high-resolution peripheral quantitative computed tomography: an exploratory study, Can. Orthop. Res. Soc. Annu. Meet, 2013.